nature biotechnology

BRIEF COMMUNICATION

https://doi.org/10.1038/s41587-020-0679-9

Deep brain optogenetics without intracranial surgery

Ritchie Chen[1,6], Felicity Gore[1,6], Quynh-Anh Nguyen[2], Charu Ramakrishnan[1], Sneha Patel[1], Soo Hyun Kim[1], Misha Raffiee[1], Yoon Seok Kim[1], Brian Hsueh[1], Esther Krook-Magnusson[3], Ivan Soltesz[2] and Karl Deisseroth[1,4,5]✉

Achieving temporally precise, noninvasive control over specific neural cell types in the deep brain would advance the study of nervous system function. Here we use the potent channelrhodopsin ChRmine to achieve transcranial photoactivation of defined neural circuits, including midbrain and brainstem structures, at unprecedented depths of up to 7 mm with millisecond precision. Using systemic viral delivery of ChRmine, we demonstrate behavioral modulation without surgery, enabling implant-free deep brain optogenetics.

Certain symptoms of neurological and psychiatric disease can be treated by modulation of pathological brain activity in both preclinical and clinical settings[1–4]. However, existing methods for neuromodulation are not cell type specific (for example, transcranial magnetic or direct current stimulation) and/or are invasive (for example, electrical deep brain stimulation)[2,3]. In basic research settings, optogenetics with microbial channelrhodopsins (ChRs) enables cell type-specific excitation or inhibition of neuronal activity with light, permitting the tuning of cellular activity in terms of levels, ratios and rhythms with improved precision, which in many cases results in symptom-relevant treatment via optical neuromodulation[4–6]. However, the delivery of visible light often requires invasive implantation of foreign materials and devices into the brain, which damages tissue and increases infection and ischemia risk[1,7]. To improve long-term biocompatibility, optogenetic effects can be recruited by light delivered external to a thinned skull[8]. However, light attenuation by scattering and absorption in bone and tissue currently limits transmission of sufficient photon densities to stimulate neural activity in deep brain structures, even with fast ChR variants engineered to respond to lower intensity and/or longer wavelengths of light for access to deeper tissue[9–11]. Engineered ChRs with slow off-kinetics (for example, stable step-function opsins) can integrate photons for modulation of distal neural populations, but cannot provide the high temporal control enabled by fast opsins[12].

We recently described the potent fast red-shifted opsin ChRmine, which exhibits extremely large photocurrents with hundred-fold improved operational light sensitivity compared with existing fast red-shifted variants and rapid off-kinetics suitable for millisecond-scale control over neural activity[13] (Supplementary Table 1)—photophysical properties that may be suitable for deep transcranial optogenetics. To determine whether ChRmine can enable safe and rapid transcranial deep brain photoactivation, we performed optically paired in vivo extracellular electrophysiology in the ventral tegmental area (VTA), 4.5 mm deep from the skull surface (Fig. 1a,b). We used ChRmine targeted to somata with a Kv2.1 peptide tag to minimize axonal localization and antidromic activation (AAV8-CamKIIα::ChRmine-oScarlet-Kv2.1; Extended Data Fig. 1a). A 400-µm fiber optic was positioned directly above the surface of the intact skull and short pulses of 635-nm light were delivered at varying pulse duration (1–100 ms), irradiance (40–1,600 mW mm^{-2} (5–200 mW)) and frequency (5–40 Hz). At 5-ms pulse width, we identified light-responsive neurons spiking in response to irradiance ≥200 mW mm^{-2}, with spiking fidelity exceeding 0.8 at power densities ≥800 mW mm^{-2} (Fig. 1c–f). Recordings with the red-shifted excitatory opsin bReaChES, which has been demonstrated to allow transcranial stimulation but exhibits lower photosensitivity and photocurrent magnitude relative to ChRmine (Supplementary Table 1)[9,11,14], yielded no light-responsive units at these depths. We found that 5–20 Hz neural activity was reliably evoked at pulse durations ≥5 ms (Extended Data Fig. 1b–i). Since increased pulse duration improved neural responsivity, we extended the pulse time to 100 ms and found that light delivered to the surface of the skull as low as 40 mW mm^{-2} reliably evoked deep VTA neural activity (Extended Data Fig. 1j–m). Spike latencies were increased at either low irradiance or short pulse durations (Fig. 1f and Extended Data Fig. 1e,m); whole-cell patch clamp in primary neural culture also revealed increased time to threshold at low irradiance (Extended Data Fig. 1n).

To test the depth limits at which we could activate ChRmine-expressing neurons with transcranial light delivery, we injected AAV8-CamKIIα::ChRmine-oScarlet-Kv2.1 at varying depths in a rat (Extended Data Fig. 2). We observed reliable photostimulation (spike probability > 0.8) down to 7 mm using 100-ms pulse widths at 400 mW mm^{-2} (Extended Data Fig. 2h–j), consistent with Monte Carlo simulations for red light transmission which revealed that ~0.02% of initial irradiance (400 mW mm^{-2}) can penetrate to these depths, near the sensitivity limit predicted for ChRmine[13] (Extended Data Fig. 3a and Supplementary Table 1). Of note, we found that these conditions, suitable for deep transcranial optogenetics, did not show evidence of tissue damage due to tissue heating or other phototoxicity effects[15,16] (Extended Data Fig. 3, Supplementary Table 2 and Supplementary Note).

To test whether deep transcranial activation of ChRmine could modulate mouse behavior, we expressed ChRmine in mesocorticolimbic dopamine neurons by injecting AAV8-EF1α::DIO-ChRmine-oScarlet into the VTA of DAT::Cre mice. After 2 weeks of expression, we tested whether transcranial

[1]Department of Bioengineering, Stanford University, Stanford, CA, USA. [2]Department of Neurosurgery, Stanford University, Stanford, CA, USA. [3]Department of Neuroscience, University of Minnesota, Minneapolis, MN, USA. [4]Department of Psychiatry & Behavioral Sciences, Stanford University, Stanford, CA, USA. [5]Howard Hughes Medical Institute, Stanford University, Stanford, CA, USA. [6]These authors contributed equally: Ritchie Chen, Felicity Gore. ✉e-mail: deissero@stanford.edu

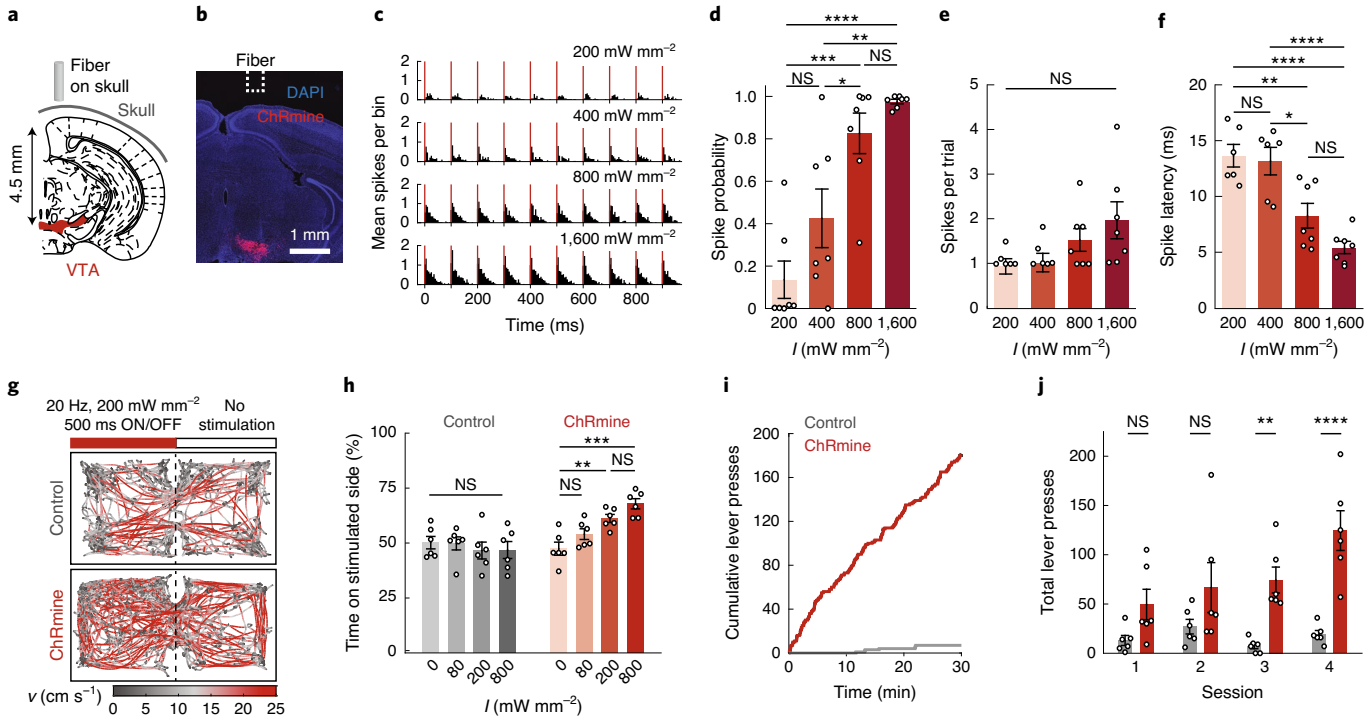

Fig. 1 | Deep transcranial photoactivation. a, Schematic depicting position of the light source relative to the targeted neural population (red) in the VTA. **b**, Confocal image of DAPI-labeled cells (blue) with neurons expressing ChRmine-oScarlet (red) in the VTA. **c**–**f**, In vivo single-unit responses following transcranial stimulation plotted as: representative peristimulus time histogram of transcranial light-evoked spikes in 5-ms bins (**c**); probability of one or more evoked spikes (**d**); number of spikes per pulse (**e**); and latency to the first spike across the population of neurons as a function of irradiance (*I*) (**f**) ($n=7$ from 2 mice; one-way ANOVA with Bonferroni post hoc tests: $F(3,24)=16.19$, $P=0.000006$ (**d**); $F(3,22)=2.11$, $P=0.13$ (**e**); and $F(3,22)=16.07$, $P=0.000009$ (**f**). Note that one neuron exhibited no spike response at 200 and 400 mW mm^{-2}, and hence there was no associated latency or spike count). **g**, Example path-tracing of a DAT-Cre mouse with oScarlet (control, gray) or ChRmine-oScarlet (red) expression during the real-time place preference test. Red bar indicates stimulation side. Tracks are color coded for velocity (*v*). **h**, Percentage of time spent on the stimulation side at varying irradiances ($n=6$ mice; one-way repeated-measures ANOVA with Bonferroni post hoc tests: $F(3,15)=10.56$, $P=0.0005$). **i**, Example cumulative lever presses performed by a ChRmine-oScarlet (red) mouse and an oScarlet (control, gray) mouse receiving transcranial stimulation. **j**, Total number of daily lever presses ($n=6$ mice; two-way repeated-measures ANOVA: control versus ChRmine $F(1,10)=26.31$, *P* value = 0.0004; with Bonferroni post hoc tests). $^*P<0.05$; $^{**}P<0.01$; $^{***}P<0.001$; $^{****}P<0.0001$; NS, not significant. Data are mean ± s.e.m.

optical stimulation could specifically modulate appetitive conditioning in the real-time place preference assay. We found that ChRmine-expressing mice spent an increased proportion of their time in the stimulation-paired zone with irradiance ≥200 mW mm^{-2} (20 Hz, 5 ms), whereas oScarlet (control) mice did not (Fig. 1g,h). The same behavior could be evoked after 6 months of chronic expression with minimal toxicity (Extended Data Fig. 4). Place preference was frequency-dependent[17], and could be generated at irradiance as low as 40 mW mm^{-2} with 100-ms pulses (Extended Data Fig. 5a,b). In addition, transcranial stimulation of the VTA reinforced operant lever-pressing behavior, with ChRmine-expressing mice performing increased numbers of daily lever presses for optical stimulation compared with control animals (Fig. 1i,j). By contrast, bReachES failed to elicit place preference even when light power was increased to 3.2 W mm^{-2} (bReachES stimulation also failed to induce VTA cFos expression; Extended Data Fig. 5c–e).

Deep transcranial photoactivation raises the possibility of exploring interventions for brain disorders where the light source is well-separated from the target cells. In epilepsy, closed-loop feedback control for seizure suppression may represent a means to avoid potentially detrimental side effects of continuous stimulation[18]. In an intrahippocampal kainic acid model of temporal lobe epilepsy, we optogenetically targeted hippocampal parvalbumin (PV)$^+$ inhibitory (GABAergic) interneurons to provide feedforward inhibition and abort focal seizures in wild-type animals[19,20] (Fig. 2a and Extended Data Fig. 6a,b). Using within-subject controls, wherein 50% of randomly selected instances of seizure onset were detected and coupled to a trigger of transcranial light delivery (40 mW mm^{-2}, 50 ms on, 100 ms off for 10 s), seizure duration was truncated by 51 ± 2% compared with sham treatment (Fig. 2b–d,g and Extended Data Fig. 6). Notably, targeting ChRmine to the broader GABAergic population of hippocampal interneurons (not just PV$^+$) suppressed seizures by only 27 ± 4%, underscoring the importance of cell subtype targeting[21] (Fig. 2e,g). Illumination in opsin-negative mice, as expected, had no effect on seizures (Fig. 2f,g).

Finally, we assessed whether transcranial deep brain neuromodulation could be achieved entirely without any surgical disruption to brain tissue using systemic viral delivery of ChRmine[10,22]. We targeted serotonergic 5-HT neurons in the dorsal raphe nucleus of the brainstem in wild-type mice via retro-orbital injection of AAVPHP.eB-Tph2::ChRmine-eYFP (Fig. 2h). Following 6 weeks of expression, we asked whether transcranial stimulation of 5-HT neurons modulated social preference in the three-chamber sociability task (Fig. 2i)[23]. Transcranial stimulation of ChRmine-expressing mice, but not control mice, increased the time spent in the social zone (800 mW mm^{-2}, 20 Hz, 5-ms pulse width, 10 s ON/OFF intervals; Fig. 2i,j). Deep transcranial activation of 5-HT neurons had no effect on novel-object interactions in the same three-chamber arena or on anxiety-related behavior in the open field test, but did induce cFos expression in the raphe of ChRmine-expressing mice (Extended

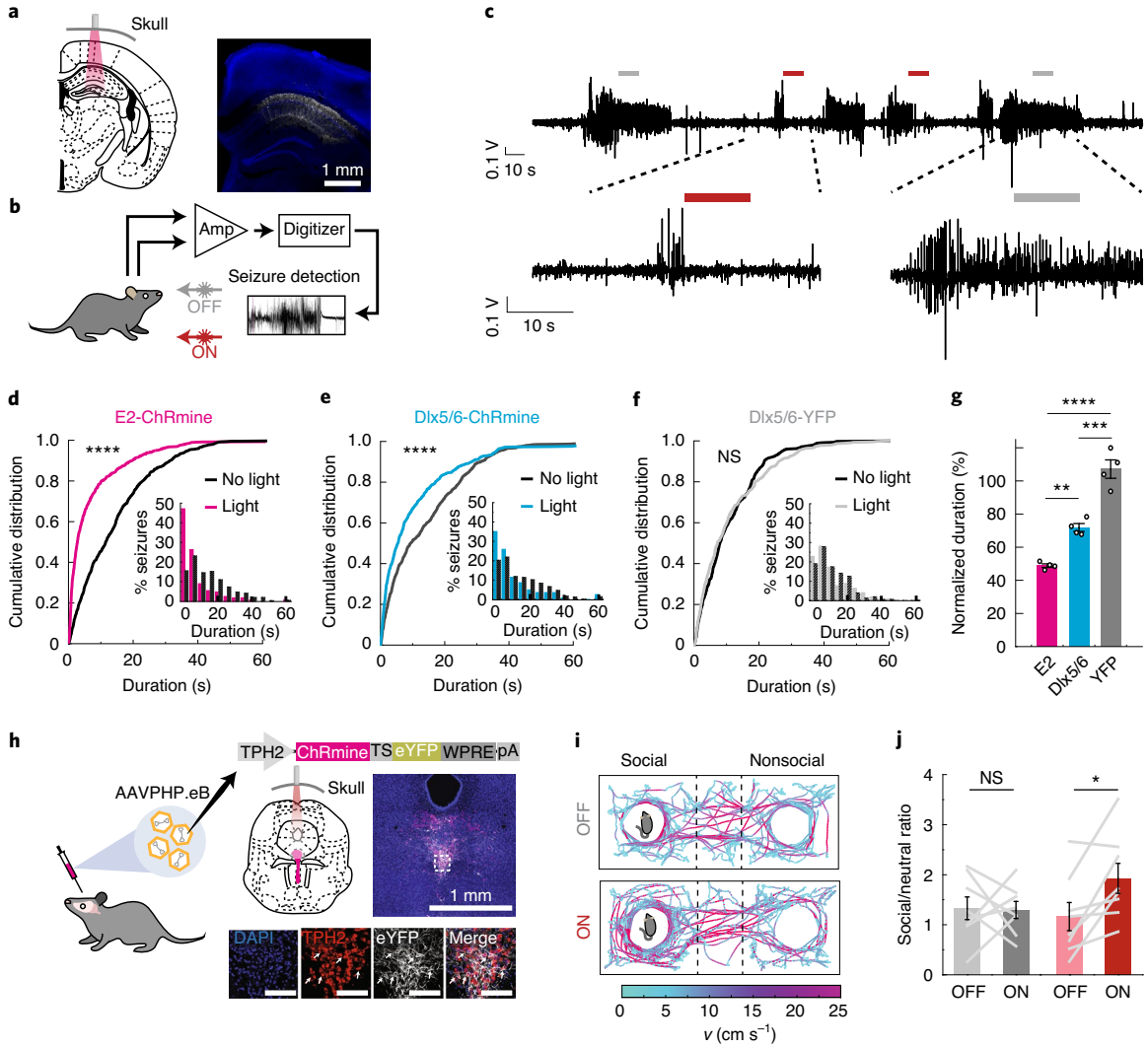

Fig. 2 | Towards deep transcranial optogenetics without cranial surgery. a, Schematic and representative confocal image of CA1 hippocampal PV neurons expressing ChRmine-YFP (white) costained with DAPI (blue). **b**, Epileptic mice were subjected to 24-h video EEG recordings, where 50% of detected seizures were set to trigger transcranial optogenetic intervention. **c**, Representative recording of electrographic seizures with no light (gray bar) or with light (red bar) treatment. **d**–**f**, Cumulative distribution and (inset) histogram of postdetection seizure duration for PV-targeted (E2-ChRmine) (**d**) and broader GABAergic-targeted (Dlx5/6-ChRmine) (**e**) or YFP control animals (**f**) (N = 1,369/1,267/1,008 seizures, respectively, n = 4 mice per group, Mann–Whitney U test). **g**, Mean seizure duration with light treatment, normalized to mean seizure duration without light treatment, for ChRmine targeted to PV GABAergic (E2), GABAergic (Dlx5/6) and control (YFP) neurons (n = 4 mice per group; one-way ANOVA with Bonferroni post hoc tests: $F(2,9) = 23.7$, $P = 0.0003$). **h**, Schematic of AAVPHP.eB-TPH2::ChRmine-eYFP systemic delivery to target serotonergic neurons in the brainstem. Confocal images depict ChRmine-YFP neurons (white), DAPI (blue) and TPH2 (red) in the raphe. White arrows denote example YFP$^+$/TPH2$^+$ neurons. Scale bar, 100 µm. **i**, Example path-tracing of a wild-type mouse from two sessions with (ON) and without (OFF) deep transcranial photostimulation during the three-chamber sociability assay. Tracks are color coded for velocity. Light at 635 nm was delivered at 20 Hz and 800 mW mm^{-2} with 5-ms pulse width over 10-s repeated intervals. **j**, Ratio of time spent in the chamber containing the juvenile mouse, relative to time spent in the empty chamber, with and without photostimulation for YFP (gray) and ChRmine-YFP (red) mice (n = 8 mice; paired t-test). *$P < 0.05$; **$P < 0.01$; ***$P < 0.01$; ****$P < 0.0001$. Data are mean ± s.e.m. Amp, amplifier.

Data Fig. 7). We found no differences in the ability to photoactivate neurons that had been targeted by systemic versus intracranial injection, despite the lower multiplicity of infection of systemic viral delivery (Extended Data Fig. 8). Taken together, these data demonstrate that deep transcranial ChRmine photoactivation can promote specific adaptive behavior without any intracranial surgery.

While existing technologies permit transcranial optogenetic manipulation of neural activity, these effects are typically restricted to superficial brain structures[9–11], lack temporal precision[12] or require stimulation parameters that substantially heat brain tissue[12]. Here we have demonstrated an approach for deep photoactivation of neurons that offers temporally precise control of spiking, exceptional depth access in a manner that can be completely non-invasive of brain tissue (overcoming the need for light-emitting implants and intracranial surgery) and minimal light power requirements. This approach for deep transcranial optogenetics was applied in multiple behavioral contexts and, with appropriate testing, may be further adapted to basic, preclinical and potentially clinical settings for fast cell type-specific neuromodulation.

Online content

Any methods, additional references, Nature Research reporting summaries, source data, extended data, supplementary information, acknowledgements, peer review information; details of

author contributions and competing interests; and statements of data and code availability are available at https://doi.org/10.1038/s41587-020-0679-9.

Received: 13 April 2020; Accepted: 21 August 2020;
Published online: 05 October 2020

References

1. Won, S. M., Song, E., Reeder, J. T. & Rogers, J. A. Emerging modalities and implantable technologies for neuromodulation. *Cell* **181**, 115–135 (2020).
2. Cagnan, H., Denison, T., McIntyre, C. & Brown, P. Emerging technologies for improved deep brain stimulation. *Nat. Biotechnol.* **37**, 1024–1033 (2019).
3. Dayan, E., Censor, N., Buch, E. R., Sandrini, M. & Cohen, L. G. Noninvasive brain stimulation: from physiology to network dynamics and back. *Nat. Neurosci.* **16**, 838–844 (2013).
4. Tye, K. M. & Deisseroth, K. Optogenetic investigation of neural circuits underlying brain disease in animal models. *Nat. Rev. Neurosci.* **13**, 251–266 (2012).
5. Yizhar, O., Fenno, L. E., Davidson, T. J., Mogri, M. & Deisseroth, K. Optogenetics in neural systems. *Neuron* **71**, 9–34 (2011).
6. Deisseroth, K. & Hegemann, P. The form and function of channelrhodopsin. *Science* **357**, eaan5544 (2017).
7. Chen, R., Canales, A. & Anikeeva, P. Neural recording and modulation technologies. *Nat. Rev. Mater.* **2**, 16093 (2017).
8. Gradinaru, V. et al. Targeting and readout strategies for fast optical neural control in vitro and in vivo. *J. Neurosci.* **27**, 14231–14238 (2007).
9. Lin, J. Y., Knutsen, P. M., Muller, A., Kleinfeld, D. & Tsien, R. Y. ReaChR: a red-shifted variant of channelrhodopsin enables deep transcranial optogenetic excitation. *Nat. Neurosci.* **16**, 1499–1508 (2013).
10. Bedbrook, C. N. et al. Machine learning-guided channelrhodopsin engineering enables minimally invasive optogenetics. *Nat. Methods* **16**, 1176–1184 (2019).
11. Zhang, F. et al. Red-shifted optogenetic excitation: a tool for fast neural control derived from *Volvox carteri*. *Nat. Neurosci.* **11**, 631 (2008).
12. Gong, X. et al. An ultra-sensitive step-function opsin for minimally invasive optogenetic stimulation in mice and macaques. *Neuron* **107**, 38–51 (2020).
13. Marshel, J. H. et al. Cortical layer–specific critical dynamics triggering perception. *Science* **365**, eaaw5202 (2019).
14. Rajasethupathy, P. et al. Projections from neocortex mediate top-down control of memory retrieval. *Nature* **526**, 653–659 (2015).
15. Stujenske, JosephM., Spellman, T. & Gordon, JoshuaA. Modeling the spatiotemporal dynamics of light and heat propagation for in vivo optogenetics. *Cell Rep.* **12**, 525–534 (2015).
16. Owen, S. F., Liu, M. H. & Kreitzer, A. C. Thermal constraints on in vivo optogenetic manipulations. *Nat. Neurosci.* **22**, 1061–1065 (2019).
17. Tsai, H.-C. et al. Phasic firing in dopaminergic neurons is sufficient for behavioral conditioning. *Science* **324**, 1080–1084 (2009).
18. Berényi, A., Belluscio, M., Mao, D. & Buzsáki, G. Closed-loop control of epilepsy by transcranial electrical stimulation. *Science* **337**, 735–737 (2012).
19. Krook-Magnuson, E., Armstrong, C., Oijala, M. & Soltesz, I. On-demand optogenetic control of spontaneous seizures in temporal lobe epilepsy. *Nat. Commun.* **4**, 1376 (2013).
20. Vormstein-Schneider, D. C. et al. Viral manipulation of functionally distinct neurons from mice to humans. *Nat. Neurosci.* https://doi.org/10.1038/s41593-020-0692-9 (2020).
21. Cho, K. K. et al. Gamma rhythms link prefrontal interneuron dysfunction with cognitive inflexibility in *Dlx5/6*$^{+/-}$ mice. *Neuron* **85**, 1332–1343 (2015).
22. Chan, K. Y. et al. Engineered AAVs for efficient noninvasive gene delivery to the central and peripheral nervous systems. *Nat. Neurosci.* **20**, 1172 (2017).
23. Walsh, J. J. et al. 5-HT release in nucleus accumbens rescues social deficits in mouse autism model. *Nature* **560**, 589–594 (2018).

Methods

Animal subjects. All experimental protocols were approved by the Stanford University Institutional Animal Care and Use Committee following the National Institutes of Health guidelines for the care and use of laboratory animals. C57BL/6J male mice at 4–8 weeks old were purchased from the Jackson Laboratory. Long-Evans male rats at 12 weeks old were purchased from Charles River. For the characterization of reward-related behaviors, we bred DAT::IRES-Cre homozygous male mice (Jackson Laboratory 006660) with wild-type C57BL/6J females. Only heterozygous male offspring back-crossed for at least five generations were used for experiments. Littermate same-sex rats were housed as pairs per cage. Mice were group-housed with two to five same-sex littermates per cage. All mice were housed on a reverse 12-h light/dark cycle maintained at 20–26 °C at 30–60% humidity and were given food and water ad libitum.

Animal surgeries and viral injections. For all surgeries, mice and rats were anesthetized with 1–3% isoflurane and placed on a heating pad in a stereotaxic apparatus (Kopf Instruments). All viruses were produced at the Stanford Neuroscience Gene Vector and Virus Core.

For mouse electrophysiology experiments, 200 nl of either rAAV8-CaMKII α::ChRmine-Kv2.1-oScarlet (5×10^{11} vector genomes (vg) per ml) or rAA V8-CaMKIIα::bReaChES-TS-p2A-mCh (1.5×10^{12} vg per ml) was unilaterally injected into the VTA at anterior-posterior (A/P) −3.3, medial-lateral (M/L) +0.4 and dorsal-ventral (D/V) −4.5 in 8–10-week-old mice. Extracellular recordings were performed within 10–21 d of expression.

For rat electrophysiology, 500 nl of rAAV8-CaMKIIα::ChRmine-Kv2 .1-oScarlet (5×10^{11} vg per ml) was injected at A/P −3, medial-lateral M/L ±4.75 and dorsal-ventral D/V −6, −7 or −8 for depth recordings at 6, 7 and 8 mm, respectively. Extracellular recordings were performed within 10–14 d of injection.

For reward-related behavioral assays in DAT::Cre mice, 500 nl of rAAV8-Ef1α::DIO-oScarlet (1×10^{12} vg per ml), rAAV8-Ef1α::DIO-ChRmine-oScarlet (1×10^{12} vg per ml) or rAAV8-Ef1α::DIO-bReaCHES-TS-eYFP (5×10^{12} vg per ml) was unilaterally injected into the VTA at A/P −3.3, M/L +0.4 and D/V −4.5 in 8-week-old mice. After 2 weeks of expression, 400-µm, 0.39-numerical aperture (NA) fibers attached to a 2.5-mm-diameter stainless steel ferrule (Thorlabs) were fixed over intact skull immediately adjacent to the injection site with Metabond (Parkell).

For experiments in epileptic mice, 1 µl of rAAV8-Dlx5/6::eYFP (2×10^{12} vg per ml), rAAV8- Dlx5/6::ChRmine-eYFP (2×10^{12} vg per ml) or rAAV8-E2::ChRmine-eYFP (2×10^{12} vg per ml) was unilaterally injected into hippocampal CA1 at A/P −2.0, M/L −1.7 and D/V −1.35 in 8-week-old mice. To induce focal seizures, 40–60 nl of kainic acid monohydrate (Sigma Aldrich (K0250); 20 mM in 0.9% NaCl) was injected into the contralateral hippocampus at A/P −2.0, M/L +1.25 and D/V −1.6 in the same mice following viral injection. After 2 weeks to allow for recurrent and spontaneous seizures to stabilize, twisted bipolar depth electrodes (PlasticsOne) were placed posteroventral to the kainic acid injection at A/P 2.5, M/L 1.75 and D/V 1.4. A 200-µm, 0.39-NA fiber attached to a 1.25-mm-diameter stainless steel ferrule was fixed over intact skull adjacent to the viral injection site. Both electrode and optical fiber were fixed in position with Metabond.

For intravascular targeting of the raphe, either rAAVPHP.eB-Tph2::eYFP or rAAVPHP.eB-Tph2::ChRmine-eYFP (4×10^{11} vg in 60 µl of 0.9% NaCl per mouse) was injected retro-orbitally in 4-week-old mice. At 8 weeks of age, 400-µm, 0.39-NA fibers attached to a 2.5 mm diameter stainless steel ferrule (Thorlabs) were fixed over intact skull at A/P 4.3 and M/L 0.

For comparison of expression and photo-responsiveness between intravascular versus intracranial targeting of Purkinje neurons, rAAVPHP. eB-L7::ChRmine-p2A-eYFP was injected either into 4-week-old mice retro-orbitally (4×10^{11} vg in 50 µl of 0.9% NaCl per mouse) or into 10–12-week-old mice intracranially (1 µl at A/P −5.7, M/L ±0.75 and D/V −3.5). Extracellular recordings were performed after 2 months (retro-orbital) or 2 weeks (intracranial) from viral injections.

In vivo electrophysiology. Mice and rats were anesthetized with 1–3% isoflurane throughout the recording session. Single units were recorded extracellularly with 32-channel count silicon probes (Cambridge Neurotech) grounded to a stainless steel screw fastened to the skull and preamplified with an RHD2132 amplifier (Intan). Electrodes were lowered through a craniotomy into the target site with a stereotax. Data acquisition was performed at 30 kHz with an Open Ephys acquisition system. A 635-nm red diode laser (CNI Optoelectronics Technology) connected to a 400-µm, 0.39-NA optical fiber was placed directly above intact skull adjacent to the craniotomy with signal output controlled by a function generator (Master-8, AMPI). For each stimulus condition three sweeps of pulses were presented, with each sweep lasting 10 s. Well-isolated single units were identified using Kilosort2 and Phy2. Spike trains were temporally downsampled to 1 kHz. Data were analyzed using custom MATLAB scripts. In 1–10-ms pulse width conditions, a light-responsive unit was defined as a neuron that reliably responded (>80% of trials) within 25 ms of light onset in the 1,600 mW mm^{-2}, 5-ms pulse width condition. In 100-ms pulse width conditions, to identify light-responsive units at increased depth, a light-responsive unit was defined as a neuron that reliably responded (>80% of trials) within 100 ms of light onset in the 400 mW mm^{-2}, 100-ms pulse width condition. For 'spikes per trial' and 'spike latency' analyses, only units with a spike probability >0 within each condition were included. For short pulse width experiments (1–10-ms pulse width), only trials with a spike in the first 25 ms after light onset were included in analysis. For long pulse width experiments (100-ms pulse width), only trials with a spike in the first 100 ms after light onset were included in analysis. Peristimulus time histograms were generated by binning data in 5-ms bins and averaging over thirty 1-s intervals.

Behavioral tests. Behavioral assays were performed during the active dark phase (10:00 to 18:00) at least 1 week after cementing of fiber optic on skull. Before tests, mice were habituated to handling for 5 d (5 min per session). Optic fibers on skull were connected to a patch cable (Doric) with a metal sleeve and connected to a 635-nm diode laser (CNI Optoelectronics Technology). A microcontroller (Arduino UNO) was used to control the output of the laser, with irradiance measured with a digital optical power meter (Thorlabs). Behavioral assays were performed by individuals blinded to the type of opsin expression. Mouse movement was tracked with EthoVision XT (Noldus).

Real-time place preference test. A 30×60 cm^2 arena was divided into left and right chambers of equal size. The test mouse was allowed to freely explore for 5 min, after which entry into one of the two sides resulted in photostimulation (repeated interval: 500 ms ON at 20 Hz, 5-ms pulse width, followed by 500 ms OFF). Animals were counterbalanced between sides paired with stimulation. Light power density (0, 80, 200, 800, 3,200 mW mm^{-2}) was randomly assigned per daily session until the testing set was completed. Movement was tracked with a video camera located above the arena and place preference was calculated by dividing the time spent in the photostimulation side by the total time of the real-time place preference assay.

Transcranial self-stimulation test. A test mouse was placed in a 20×20 cm^2 chamber with a lever (Coulbourn Instruments) extended into the chamber. A single press of the lever resulted in 3-s photostimulation (5-ms pulse width, 20 Hz, 50 mW, 10% duty cycle) with a 10-s timeout following rewarded lever press. Reinforcement learning was assessed by measuring the number of lever presses performed over five daily sessions lasting 30 min, with no photostimulation received during lever press in the first session. The lever press box signal was digitized with a DAQ device (National Instruments) and recorded with custom MATLAB scripts.

Three-chamber sociability and novel-object test. We based our three-chamber task on a design described previously[24], with two compartments (32×32 cm^2) separated by a smaller middle compartment (32×10 cm^2). The left and right compartments each contained an inverted wire cup. For habituation, mice were allowed to freely explore the experimental arena for 5 min before social tests, after which a juvenile male (4–5 weeks old) was placed in one of the two inverted cups. The test mouse was then allowed to explore the compartments for an additional 10 min. This test was repeated 24 h later using a different juvenile mouse (counterbalanced between days 1 and 2). During the social assay in which the juvenile mouse was present, the test mouse received optical stimulation (5-ms pulse width at 20 Hz and 100 mW for 10 s, with 10 s off, repeated during the duration of the test) on 1 of the 2 days (counterbalanced between days 1 and 2). Movement was tracked with a video camera located above the arena and the social/nonsocial ratio was calculated by dividing the time spent in the zone containing the juvenile mouse by the time spent in the opposing chamber. Novel-object preference tests were conducted a week after conclusion of the social assays. These tests were conducted similarly except the juvenile mouse was substituted with a novel object.

Open field test. To assess for anxiety-related behavior, mice were placed in a 60×60 cm^2 arena and allowed to freely explore for 15 min. During the middle 5-min epoch, 635-nm light was delivered (800 mW mm^{-2}, 20 Hz and 5-ms pulse width). Movement was tracked with a video camera positioned above the arena. The central region of the chamber was defined as 48×48 cm^2.

Closed-loop seizure detection and transcranial optogenetics. Closed-loop seizure detection and on-demand light delivery were performed as previously described. Briefly, a seizure detection MATLAB script that identified spike features was used to analyze hippocampal electroencephalogram (EEG) signal in real-time[25]. Upon seizure detection, there was a 50% chance each seizure would receive either transcranial photostimulation or no light in random sequence. Light delivery consisted of a 10-s bout (50 ms on/100 ms off) delivered at 5 mW. After light delivery, another light stimulation was prevented for the next 60 s to avoid overstimulation. EEG signals associated with each trigger were analyzed offline by individuals blinded to the light condition used. Seizure duration was quantified by subtracting the detection dwell time (typically 1–3 s) from the total duration of the electrographic seizure.

Tissue histology. Following injection with sodium pentobarbital (200 mg kg^{-1}; intraperitoneally) to induce deep anesthesia, mice and rats were transcardially perfused with ice-cold PBS followed by 4% paraformaldehyde in PBS. Excised brains were then fixed overnight in 4% paraformaldehyde at 4 °C on a shaker.

The following day, 65-µm-thick slices were prepared with a microtome and subsequently stored in cryoprotectant at −20 °C. Before staining, slices were washed in 1× phosphate buffer saline with 0.1% Triton-X100 (PBST) for 1 h. For immunostaining, sections were blocked in 5% normal donkey serum (Jackson ImmunoResearch) in PBST for 30 min at room temperature followed by incubation with primary antibody: rabbit anti-cFos (1:200; abcam no. ab214672), or rabbit anti-Iba1 (1:200; Wako) and chicken anti-GFAP (1:500; abcam no. ab4674) overnight at 4 °C. Sections were subsequently washed two times in PBST (30 min each) and then transferred to a secondary antibody solution: AffiniPure F(ab')$_2$ Fragment donkey anti-rabbit 647 or donkey anti-chicken-488 (1:500; Jackson ImmunoResearch) for 3 h at room temperature. Sections were washed three times in PBST (30 min each). For nuclei staining, slices were incubated in PBST with 4′,6-diamidino-2-phenylindol (DAPI; 1:25,000) for 30 min after incubation with secondary antibodies and washed three times in PBST (30 min each).

Protocols for in situ RNA detection were adapted from the third-generation hybridization chain reaction protocols[26]. Probes for VGAT, PV, tryptophan hydroxylase 2 (TPH2) or cFos were designed with the split initiator approach to eliminate the need for probe optimization and to suppress background signal. Even and odd 22–25-nucleotide antisense oligo pairs carrying split B1 or B5 initiation sequences were tiled across the length of the exon sequence for the gene of interest and synthesized by IDT and used without further purification. Dye-conjugated hairpins (B1-647, B5-546) were purchased from Molecular Technologies. Hybridizations with split probes were performed overnight in 2× SSCT, 10% (v/v) dextran sulfate and 10% (v/v) formamide at 4-nM probe concentration. The next day, slices were washed (three times in 2× saline-sodium citrate with 0.1% Triton-X100 (SSCT), 10% (v/v) formamide at 37 °C then two times in 2× SSCT at room temperature; 20 min each) and then incubated in amplification buffer (5× SSCT, 10% (v/v) dextran sulfate). During this time, dye-conjugated hairpins were heated to 95 °C for 1 min then snap-cooled on ice. Hairpin amplification was performed by incubating individual slices in 50 µl of amplification buffer with B1 and B5 probes at concentrations of 240 nM overnight in the dark. Samples were stained with DAPI, washed three times with 5× SSCT for 30 min each and then imaged.

Simulation of laser transmission and heating in tissue. Light transmission and tissue heating were calculated using freely available published code that used Monte Carlo simulations of light propagation coupled to Penne's bioheat equation[15]. The laser parameters and calculated maximum temperature change are presented in Supplementary Table 2. We assumed steady-state temperature changes to be reached after 2 min of simulation, based on calculated temperature profiles reaching maximum values within tens of seconds.

Statistics and reproducibility. Group comparisons were made using one-way or two-way analysis of variance (ANOVA) followed by Bonferroni post hoc tests to control for multiple comparisons. Two-tailed *t*-tests were used to make single-variable comparisons. A two-tailed Mann–Whitney *U* test was used to compare seizure duration distribution for light and no-light conditions at the individual and group levels, where animals were grouped by targeted cell type. All histology experiments on mice and rats were performed on three or more different animals with similar results. Histology analysis was performed with ImageJ 1.52. Statistical analysis was done using MATLAB R2019b, GraphPad Prism 8 or Origin 2020. A P value <0.05 was considered significant.

Reporting Summary. Further information on research design is available in the Nature Research Reporting Summary linked to this article.

Data availability

The data that support the findings of this study are available upon reasonable request.

Code availability

Analysis code will be made available upon reasonable request.

References

24. Matthews, G. A. et al. Dorsal raphe dopamine neurons represent the experience of social isolation. *Cell* **164**, 617–631 (2016).
25. Armstrong, C., Krook-Magnuson, E., Oijala, M. & Soltesz, I. Closed-loop optogenetic intervention in mice. *Nat. Protoc.* **8**, 1475–1493 (2013).
26. Choi, H. M. et al. Third-generation in situ hybridization chain reaction: multiplexed, quantitative, sensitive, versatile, robust. *Development* **145**, dev165753 (2018).

Acknowledgements

We thank C. Bedbrook, M. Lovett-Barron and L. Tan for feedback on the manuscript and the entire Deisseroth laboratory for advice and discussions. We also thank T. Gschwind for assistance with EEG analysis. This research was supported by grants from the NIH, NSF, Gatsby, Fresenius, Wiegers, Grosfeld and NOMIS Foundations (to K.D.); a Walter V. and Idun Berry Postdoctoral Fellowship, and grant K99 DA050662 (to F.G.); a NARSAD Young Investigator Grant (to R.C. and to F.G.); grant F32 NS106764 (to Q.A.N.); grants R01 NS112518 and R01 NS104071 and the University of Minnesota's MnDRIVE (Minnesota's Discovery, Research and Innovation Economy) initiative (to E.K.-M.); and grant NS94668 (to I.S.).

Author contributions

R.C. and K.D. designed the experiments and wrote the paper with comments from all other authors. F.G. performed electrophysiology experiments and analysis. R.C. and Q.A.N. performed closed-loop EEG and optogenetic experiments and analysis with input from E.K.-M. and I.S. R.C., F.G., Q.A.N., S.P., S.H.K., M.R. and B.H. performed animal surgeries, behavior, behavioral analysis and histology. Y.S.K. performed patch clamp recordings and analysis. C.R. designed and generated constructs for viruses. K.D. supervised all aspects of the work.

Competing interests

The authors declare no competing interests.

Additional information

Extended data is available for this paper at https://doi.org/10.1038/s41587-020-0679-9.

Supplementary information is available for this paper at https://doi.org/10.1038/s41587-020-0679-9.

Correspondence and requests for materials should be addressed to K.D.

Reprints and permissions information is available at www.nature.com/reprints.

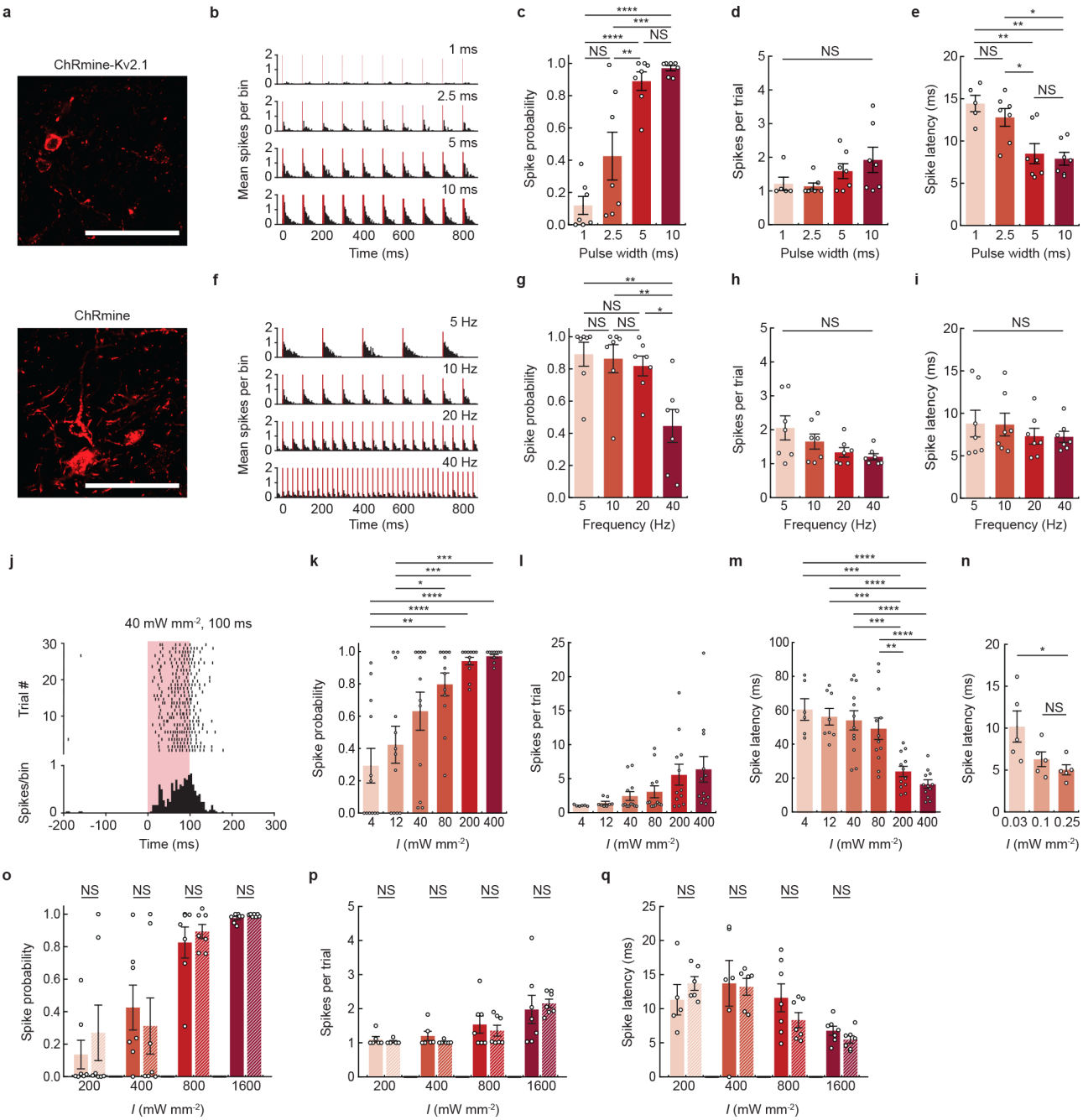

Extended Data Fig. 1 | See next page for caption.

Extended Data Fig. 1 | Extracellular electrophysiological characterization of transcranial deep brain optogenetics at different photostimulation parameters in mice. a, Confocal image of representative neurons in the VTA expressing either soma-localized (Kv2.1) or non-localized ChRmine-oScarlet. Scale bar: 100 μm. **b**, Representative peristimulus time histogram of transcranial light-evoked spikes at different pulse widths. Light-responsive single-unit neural recordings at different pulse widths plotted as: probability of one or more evoked spikes (**c**), number of spikes per pulse (**d**), and latency to the first spike (**e**) (n = 7 units from 2 mice; one-way ANOVA with Bonferroni post hoc tests: $F(3,24) = 22.51$, $P = 0.0000004$ (**c**); $F(3,22)=2.10$, $P= 0.13$ (**d**); and $F(3,22) = 9.30$, $P = 0.0004$ (**e**). Note two neurons exhibited no spike response at 1-ms pulse width and therefore do not have an associated latency or spike count at this pulse width). **f**, Representative peristimulus time histogram of transcranial light-evoked spikes at different frequencies. Light-responsive single-unit neural recordings at different frequencies plotted as: probability of one or more evoked spikes (**g**), number of spikes per pulse (**h**), and latency to the first spike (**i**) (n = 7 from 2 mice; one-way ANOVA with Bonferroni post hoc tests: $F(3,24) = 6.31$, $P = 0.003$ (**g**); $F(3,24) = 2.82$, $P = 0.06$ (**h**); and $F(3,24)=0.52$, $P = 0.67$ (**i**)). **j**, Representative raster plot and peristimulus time histogram of transcranial light-evoked spikes at low light power (40 mW mm^{-2}, 100 ms duration). Light-responsive single-unit neural recordings at different irradiance (I) with an extended pulse width of 100 ms plotted as: probability of one or more evoked spikes (**k**), number of spikes per pulse (**l**), and latency to the first spike (**m**) (n = 12 units from 2 mice; one-way ANOVA with Bonferroni post hoc tests: (**k**) $F(5,66) = 10.46$, $P = 0.0000002$ (**l**) $F(5,56) = 2.81$, $P = 0.02$, and (**m**) $F(5,56) = 14.08$, $P = 0.000000006$. Note six (4 mW mm^{-2}) and four (12 mW mm^{-2}) neurons exhibited no spike response and therefore do not have an associated latency or spike count at these irradiances). **n**, Latency to first spike determined from patch recordings of cultured hippocampal neurons at low irradiance exhibiting increased time to fire action potentials with decreasing photon density (n = 5 neurons, one-way ANOVA with Bonferroni post hoc tests: $F(2,12) = 36$, $P = 0.03$). Light-responsive single-unit neural recordings at different irradiance for ChRmine-expressing neurons with (nonstriped) or without (striped) the Kv2.1 peptide tag:probability of one or more evoked spikes (**o**), number of spikes per pulse (**p**), and latency to the first spike (**q**) (n = 7 units from 2 mice (ChRmine) and n = 7 units from 2 mice (ChRmine-Kv2.1); two-way ANOVA with Bonferroni post hoc tests: ChRmine-Kv2.1 vs ChRmine (**o**) $F(1,48)=0.02$, $P=0.88$, (**p**) $F(1,43)=0.08$, $P=0.78$, and (**q**) $F(1,43)=0.42$, $P=0.52$). No differences in the ability to photoactivate neurons with or without the Kv2.1 tag was observed. In **b**–**e**, 635 nm light was delivered at 10 Hz and 800 mW mm^{-2} light power at different pulse width. In **f**–**i**, 635 nm light was delivered at 800 mW mm^{-2} mW light power with 5-ms pulse width at different frequencies. In **j**–**m**, 635 nm light was delivered at 1 Hz with 100 ms pulse at different irradiance. $^{*}P < 0.05$; $^{**}P < 0.01$; $^{***}P < 0.001$; $^{****}P < 0.0001$; NS, not significant. Data are mean ± sem.

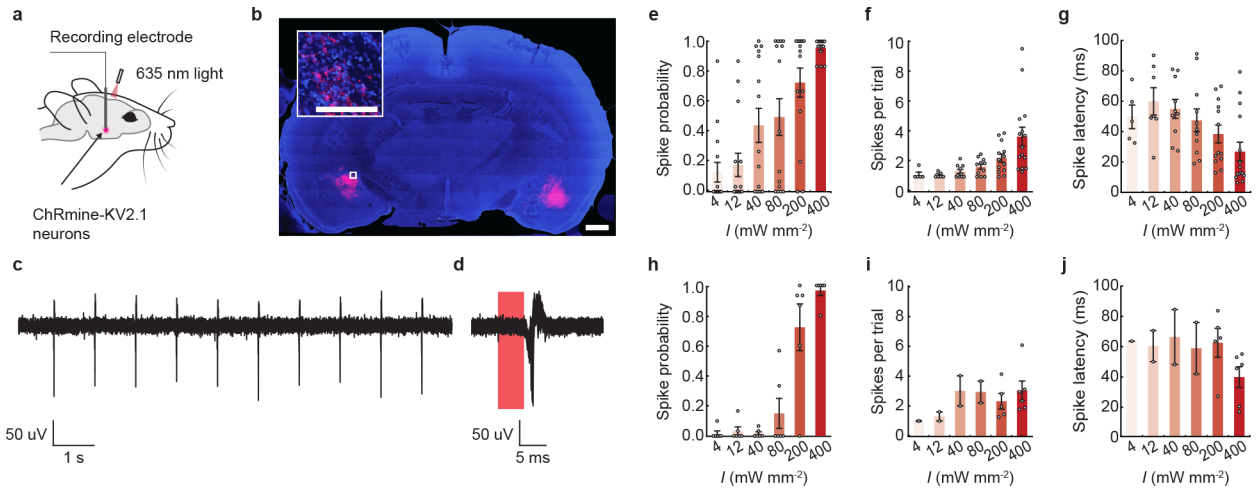

Extended Data Fig. 2 | ChRmine photoactivatable up to 7 mm from the skull. a, Schematic of experiment for extracellular recording in anesthetized rats. **b**, Confocal image of a coronal slice from rat depicting DAPI-stained cells (blue) and soma-localized ChRmine-oScarlet-Kv2.1 (red) expression in neurons at 6 mm (left) and 7 mm (right). Inset: expanded view of neurons expressing ChRmine. Scale bar: 1 mm, (inset) 100 μm. **c**, **d**, Example voltage trace of light-evoked activity in response to 5-ms pulse width of light delivered at 10 Hz with a 635 nm laser at 800 mW mm^{-2}. Light-responsive single-unit neural recordings at 6 mm plotted as: probability of one or more evoked spikes (**e**), number of spikes per pulse (**f**), and latency to the first spike (**g**) (n = 15 units from 2 rats). Light-responsive single-unit neural recordings at 7 mm plotted as: probability of one or more evoked spikes (**h**), number of spikes per pulse (**i**), and latency to the first spike (**j**) (n = 6 units from 2 rats). In **e**–**g** and **h**–**j**, 635 nm light was delivered at 1 Hz with a pulse width of 100 ms at different irradiance (*I*). At 400 mW mm^{-2}, these conditions resulted in a spike probability of 0.96 with an average spike latency of 27 ± 6 ms and a spike count of 3.7 ± 0.6 recorded at 6 mm in depth, and a spike probability of 0.97 with an average spike latency of 39 ± 7 ms and a spike count of 3 ± 0.6 at 7 mm in depth. At the same conditions, no light-evoked activity was recorded at 8 mm deep across 2 rats. Data are mean ± sem.

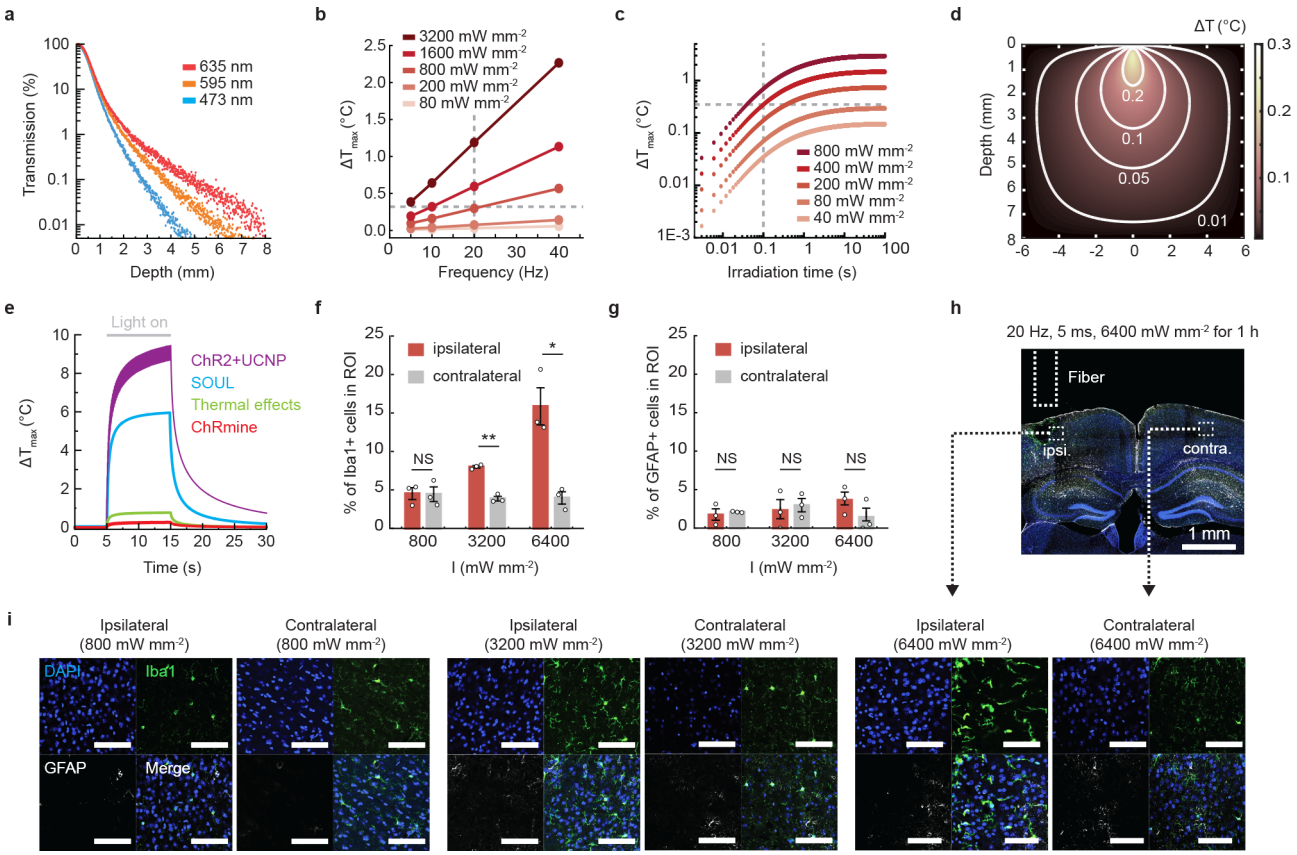

Extended Data Fig. 3 | ChRmine enabled transcranial deep brain optogenetics at light powers that elicit minimal tissue heating. a, Light transmission profile through brain tissue from a 400-μm 0.39 NA optical fiber calculated from Monte Carlo simulations of photon propagation. **b**, Calculated maximum temperature change associated with a 635 nm laser delivered at various light powers and frequencies with a pulse width of 5 ms. Note conditions used for transcranial optogenetics in mice (800 mW mm^{-2} and up to 10% duty cycle) resulted in minimal tissue heating at steady state (~0.3 °C, gray dashed line). **c**, Calculated maximum temperature change associated with a 635 nm laser delivered at various light powers as a function of continuous irradiation time. Note conditions used for transcranial optogenetics in rats (400 mW mm^{-2} with 100-ms pulse width at 1 Hz) resulted in minimal tissue heating at steady state (~0.4 °C, gray dashed line). **d**, Modeled temperature distribution in brain tissue at steady state for 635 nm light delivered at 800 mW mm^{-2}, 20 Hz, 5-ms pulse width. **e**, Calculated maximum temperature change for various laser parameters used for transcranial optogenetics applied for 10 s (see Supplementary Table 2 for summary of parameters). Note stimulation conditions for ChRmine (red) heat tissue less than range reported to have nonspecific temperature effects on behavior (green, 532 nm 222 mW mm^{-2}). Percentage of Iba^{+} microglia (**f**) and GFAP^{+} astrocytes (**g**) among DAPI-labeled cells within 200 μm of fiber optic source on the photostimulated (ipsilateral, red) or non-photostimulated (contralateral, gray) side. 635 nm light was delivered at 20 Hz with 5 ms pulse at different light powers (800, 3200, and 6400 mW mm^{-2}) for 1 hour. Animals were perfused 24 hours after photostimulation. No glial accumulation was evident at 800 mW mm^{-2} and 10% duty cycle conditions (n = 3 mice; two-sided paired t-test, $^{*}P = 0.03$; $^{**}P = 0.005$; NS, not significant). **h**, Representative confocal image depicting a coronal slice treated at 6400 mW mm^{-2} exhibiting tissue lesioning on the ipsilateral side. **i**, Representative confocal images with indicated side of photostimulation and irradiance. Scale bar: 100 μm. Data are mean ± sem.

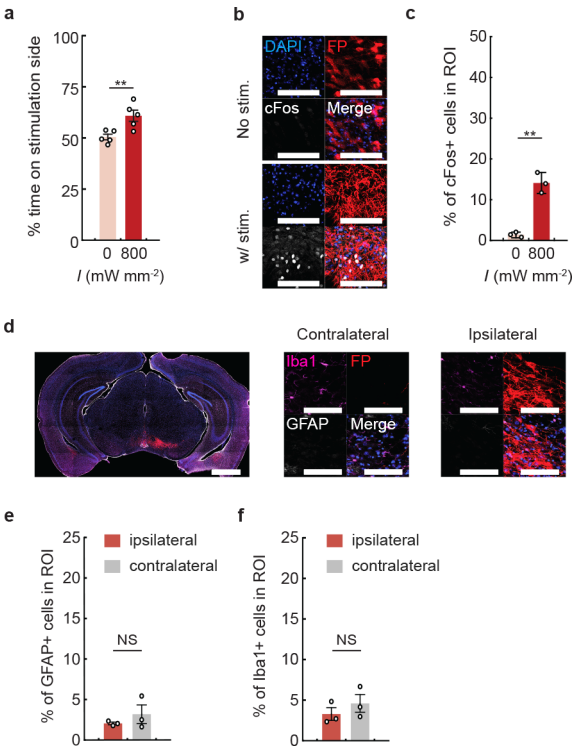

Extended Data Fig. 4 | Evaluation of long-term expression of ChRmine at 7 months. a, DAT-Cre mice following 7 months of ChRmine-oScarlet expression were subjected to a real-time place preference test with stimulation parameters at 800 mW mm^{-2}, 500 ms ON/OFF at 20 Hz with 5-ms pulse width (5% duty cycle) (n = 5 mice; two-sided paired t-test, $P = 0.003$). **b**, Representative images of cFos expression with (bottom) or without (top) stimulation. Scale bar: 100 µm. **c**, Percentage of cFos$^+$ cells among DAPI-labeled cells in the VTA. Mice were sacrificed 90 minutes following 10 minutes of transcranial photostimulation at 0 or 800 mW mm^{-2} laser delivered at 20 Hz and 5-ms pulse width (n = 3 per group; two-sided unpaired t-test, $P = 0.001$). **d**, Representative confocal image of neurons in the VTA expressing ChRmine-oScarlet (red fluorescent protein (FP)), stained with DAPI (blue, separate channel not shown), Iba1+ microglia (magenta), and GFAP+ astrocytes (white) used to assess glia distribution within the injection (ipsilateral) and contralateral side. Scale bar: 1 mm and 100 µm. Percentage of astrocytes (**e**) and microglia (**f**) among DAPI-labeled cells. No statistical difference in glial accumulation was observed in the VTA with (ipsilateral) or without (contralateral) local ChRmine expression (n = 3 per group; two-sided unpaired t-test, $P = 0.38$ (**e** and **f**)). $^{**}P < 0.01$; NS, not significant. Data are mean ± sem.

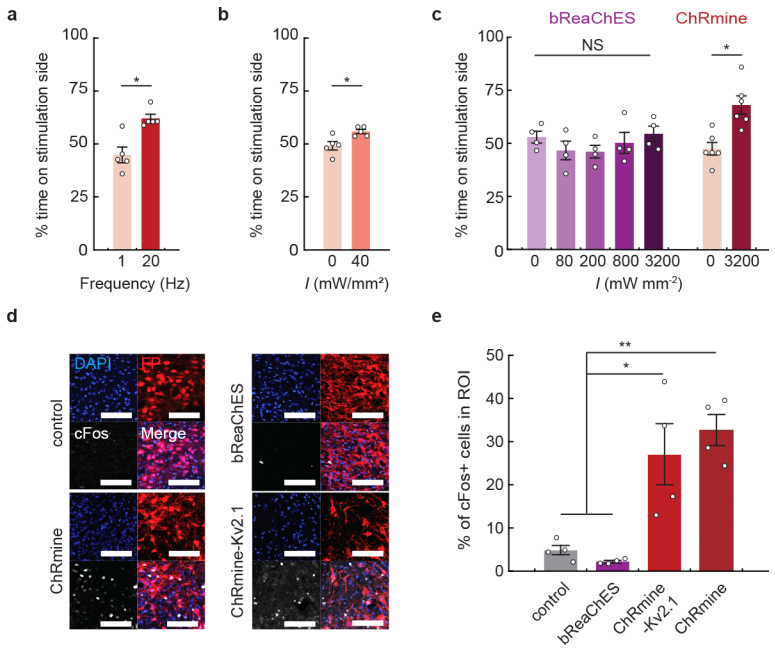

Extended Data Fig. 5 | Transcranial photoactivation of ChRmine enabled functional control of dopaminergic neurons. DAT-Cre mice with ChRmine-oScarlet expression in dopaminergic neurons were subjected to a real-time place preference test. Percent of time spent on the stimulation side receiving transcranial photostimulation with the following parameters: **a**, tonic (1 Hz) or phasic (20 Hz) stimulation delivered at 800 mW mm^{-2} and 5-ms pulse width; **b**, with and without stimulation at 40 mW mm^{-2} delivered at 5 Hz with 100-ms pulse width (n=5 mice; two-sided paired t-test, $P = 0.018$ (**a**); $P = 0.023$ (**b**)). **c**, DAT-Cre mice expressing bReaChES did not exhibit place preference even at irradiance (I) of 3200 mW mm^{-2}, 500 ms ON/OFF, 20 Hz and 5-ms pulse width (n = 4 mice (bReaChES), n = 6 mice (ChRmine); one-way repeated-measure ANOVA: $F(4,12)=1.15$, $P = 0.38$ (bReaChES) and two-sided paired t-test (ChRmine), $P = 0.02$). **d**, Representative confocal images of neurons in the VTA expressing red fluorescent protein and/or the indicated opsin (red) stained with DAPI (blue) and cFos (white). Scale bar: 100 μm. **e**, Percentage of cFos^{+} cells among DAPI-labeled cells in the VTA following 10 minutes of transcranial photostimulation at 20 Hz and 800 mWmm^{-2} with 5-ms pulse width. Animals were sacrificed after 90 minutes (n = 4 per group; one-way ANOVA with Bonferroni post hoc tests: $F(3,12) = 14.24$, $P = 0.0003$). $^{*}P < 0.05$; $^{**}P < 0.01$; NS, not significant. Data are mean ± sem.

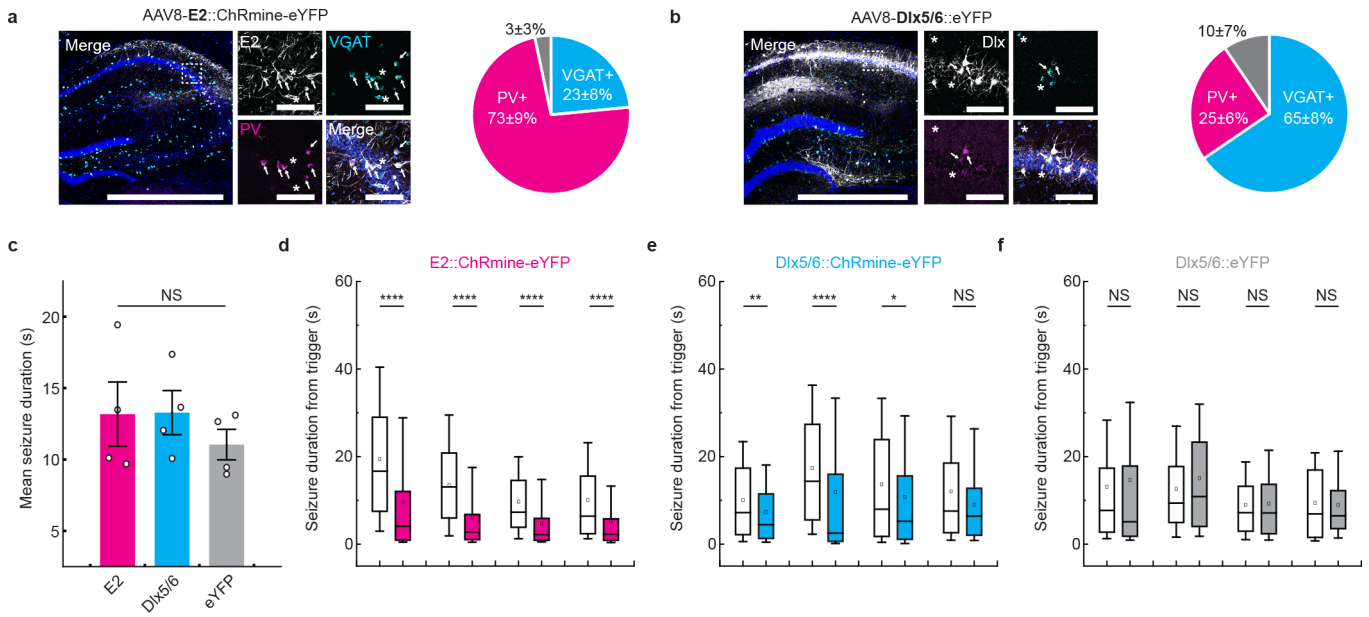

Extended Data Fig. 6 | Evaluation of cell type specificity for seizure inhibition. Representative confocal image of the hippocampus depicting ChRmine-YFP (white) neurons co-stained with DAPI (blue), the vesicular GABA transporter VGAT (cyan), and parvalbumin PV (magenta) regulated by either the E2 enhancer derived from the Scna1 gene (**a**) or the Dlx5/6 enhancer (**b**). Scale bar: 1 mm and (expanded view) 100 μm. White arrows point to YFP$^+$/VGAT$^+$/PV$^+$ neurons while proximal '*' indicate YFP$^+$/VGAT$^+$/PV$^-$ neurons. Pie chart depicts quantification of YFP$^+$ cells regulated by the E2 (**a**) or Dlx5/6 (**b**) enhancer that are either eYFP$^+$/VGAT$^+$/PV$^+$ (magenta), eYFP$^+$/VGAT$^+$/PV$^-$ (cyan), or eYFP$^+$/VGAT$^-$/PV$^-$ (grey). Note all PV$^+$ neurons were also VGAT$^+$ and that a subset of YFP$^+$ neurons (3% (E2) and 10% (Dlx5/6)) were not labeled by the VGAT GABAergic marker. A total of 302 and 227 neurons were counted from 3 (E2) and 4 (Dlx5/6) mice respectively. **c**, Comparison of mean seizure distribution without light stimulation showed comparable seizure duration across cohorts (n = 4 per group; one-way ANOVA: $F(2,9)=0.56$, $P = 0.59$). Data are mean ± sem. Box plot of each animal from E2::ChRmine-eYFP (**d**), Dlx5/6::ChRmine-eYFP (**e**) and Dlx5/6::eYFP (**f**) cohorts depicting seizure duration from trigger with (filled) and without (not filled) light treatment (n = 4 mice per group; two-sided Mann-Whitney U Test). Each box denotes lower (25%) and upper (75%) quartile with median (line) and mean (square) and whiskers depict the 10-90% range for all measured seizures. *$P < 0.05$; **$P < 0.01$; ***$P < 0.01$; ****$P < 0.0001$; NS, not significant.

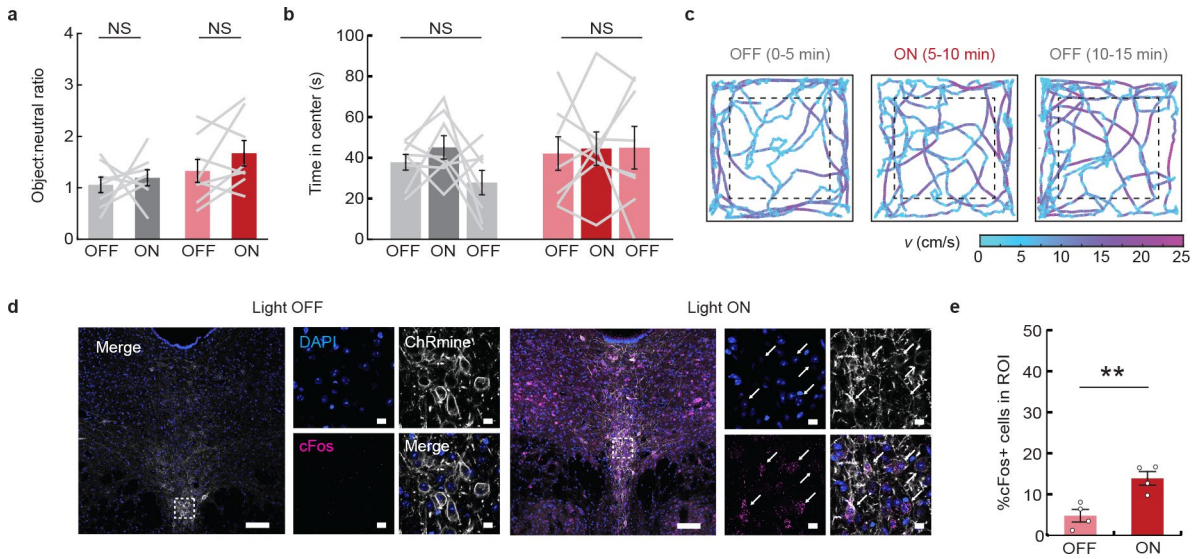

Extended Data Fig. 7 | Effects of brain-noninvasive transcranial activation of 5-HT neurons on novelty preference, anxiety-related behaviors, and induction of the neural activity marker cFos. a, Mice were assessed for novelty preference by quantifying ratio of time spent in the chamber containing a novel object relative to time spent in the empty chamber with and without photostimulation for YFP (gray) and ChRmine-eYFP (red) mice. Stimulation does not alter novel object interaction (n = 8 mice; two-sided paired t-test). **b**, Mice were assessed for anxiety-related behavior with a 15 min open field test, where the first and last 5 min block were not paired with light stimulation (OFF), while the middle 5 min was paired with 635 nm stimulation (800 mW mm^{-2}, 20 Hz, 5-ms pulse width repeated in 10 s intervals). Stimulation does not alter anxiety-behavior based on time spent in the center of the arena. (n = 8 mice; repeated-measure one-way ANOVA: $F(2,14) = 2.23$, $P = 0.15$ (eYFP) and $F(2,14) = 0.05$, $P = 0.83$ (ChRmine-eYFP)). **c**, Example path-tracing of a 5-HT ChRmine-YFP mouse during the 3 5-min blocks of the 15 min long open field test. Tracks are color coded for velocity (v). **d**, Representative confocal image of ChRmine-YFP neurons (white) in the raphe stained for cFos (magenta) by *in situ* hybridization and DAPI (blue). White arrows point to example $YFP^+/cFos^+$ neurons. Scale bar: 100 μm and (expanded view) 10 μm. **e**, Percentage of $cFos^+$ cells among DAPI-labeled cells in the raphe following 10 min of transcranial photostimulation at 20 Hz and 800 mW mm^{-2} with 5-ms pulse width. (n = 4 per group; one-way ANOVA: $F(1,6)=16$, $P = 0.007$). $^{**}P < 0.01$; NS, not significant. Data are mean ± sem.

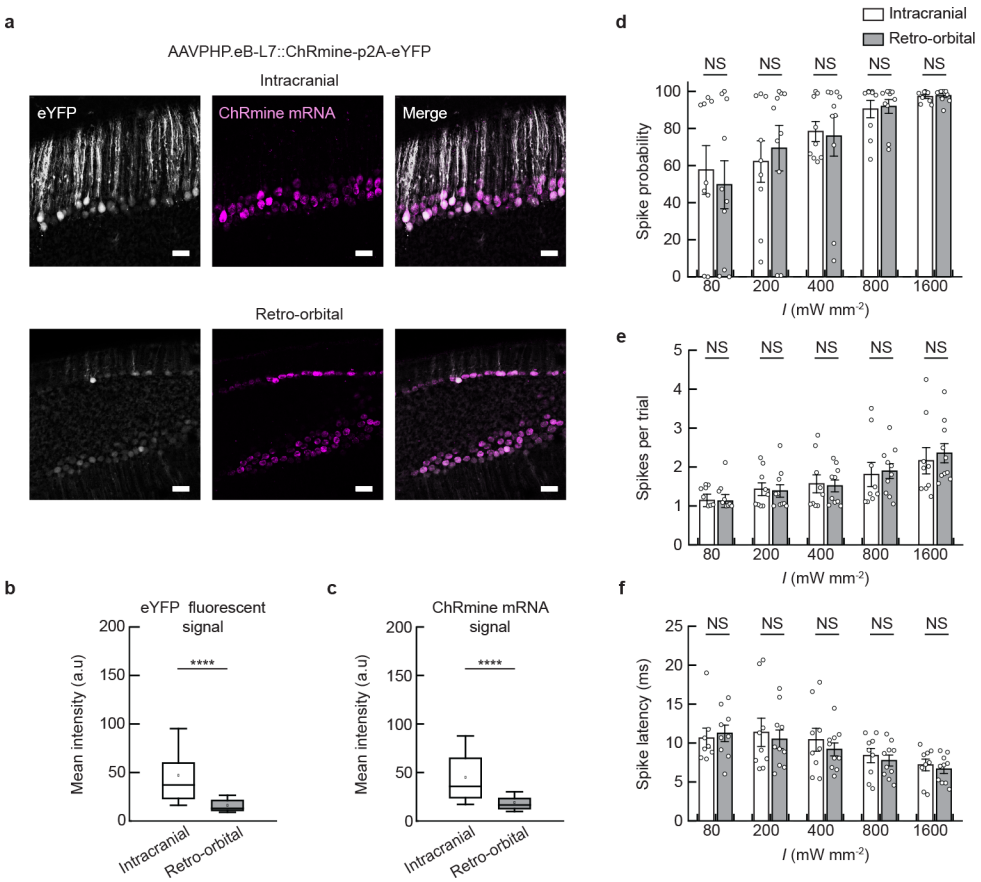

Extended Data Fig. 8 | Comparison of expression level and photoactivity of ChRmine-expressing neurons targeted by intracranial or retro-orbital delivery. a, Confocal images of Purkinje neurons expressing eYFP (white) co-labeled with *in situ* hybridization for ChRmine mRNA (magenta). Neurons were targeted by AAVPHP.eB-L7::ChRmine-p2a-eYFP by direct or retro-orbital injection. Scale bar: 100 μm. Box plot of mean intensity signal from individual neurons for (**b**) eYFP and (**c**) ChRmine mRNA (n = 2 mice, 60 neurons per group; two-sided unpaired t-test, $P = 6.7e\text{-}10$ (eYFP), 5.2e-10 (ChRmine mRNA)). The mean signal of neurons targeted by retro-orbital injection was 42% (eYFP) and 34% (ChRmine mRNA) relative to the signal from direct injection, indicative of the lower multiplicity of infection. Each box denotes lower (25%) and upper (75%) quartile with median (line) and mean (square) and whiskers depict the 10-90% range for neurons quantified. *In vivo* extracellular recordings at 3 mm from skull following transcranial stimulation from neurons expressing ChRmine targeted by intracranial (not filled) or retro-orbital (gray) injections plotted as: probability of one or more evoked spikes (**d**); number of spikes per pulse (**e**); and latency to the first spike (**f**) across the population of neurons as a function of irradiance (*I*) delivered at 10 Hz with 5-ms pulse width. No statistically significant difference was observed in single-unit response between the viral delivery methods (n = 9 units from 2 mice (intracranial) and n = 10 units from 2 mice (retro-orbital); two-way ANOVA with Bonferroni post hoc tests: intracranial vs. retro-orbital $F(1,85) = 0.002$, $P = 0.96$ (**d**); $F(1,83) = 0.05$, $P = 0.82$ (**e**) and $F(1,83) = 0.65$, $P = 0.42$ (**f**). Note one neuron in each group exhibited no spike response at 80 mW mm^{-2} and as such has no corresponding spike count or latency at this irradiance). ****$P < 0.0001$; NS, not significant. Data are mean ± sem.